Metastability of Amorphous Silicon from Silicon Network Rebonding

R. Biswas,[1] B. C. Pan,[1,2] and Y. Y. Ye[1,3]
[1]*Department of Physics and Astronomy, Microelectronics Research Center, and Ames Laboratory, Iowa State University, Ames, Iowa 50011*
[2]*Department of Physics, University of Science and Technology of China, Hefei 230026, People's Republic of China*
[3]*Center of Analysis and Testing, Wuhan University, Wuhan, People's Republic of China*
(Received 1 August 2001; published 2 May 2002)

We propose a network rebonding model for light-induced metastability in amorphous silicon, involving bonding rearrangements of silicon and hydrogen atoms. Nonradiative recombination breaks weak silicon bonds and generates dangling bond–floating bond pairs, with very low activation energies. The transient floating bonds annihilate, generating local hydrogen motion. Charged defects are also found. Support for these processes is found with tight-binding molecular dynamics simulations. The model accounts for major experimental features of the Staebler-Wronski effect including electron-spin resonance data, the $t^{1/3}$ kinetics of defect formation, two types of metastable dangling bonds, and hysteretic annealing.

DOI: 10.1103/PhysRevLett.88.205502 PACS numbers: 61.43.Dq, 71.55.Jv, 78.30.Ly

Hydrogenated amorphous silicon (a-Si:H), a material with several technological applications, suffers from the well-known light-induced degradation or the Staebler-Wronski (SW) effect. Since its initial discovery [1], the basic scientific understanding of light-induced degradation has been intensively studied [2]. In the SW effect, illumination of the material generates metastable silicon dangling bonds with midgap electronic states between 10^{16}–10^{17} cm^{-3} that degrade the transport properties and decrease solar cell efficiencies. The metastable defects can be annealed out at temperatures between 170–200 °C. Despite extensive experimental characterization, the microscopic origin of the SW effect is still debated.

Since H motion becomes important near defect annealing temperatures, H motion has been associated with defect annealing. A conclusive resolution of the atomistic mechanisms of the SW effect will have far-reaching implications for improving the stability and efficiency of solar cells and in resolving many conflicting experiments. The understanding of metastability will be of fundamental importance to glassy systems with light-induced changes.

Electron-spin resonance (ESR) of a-Si:H demonstrated that the metastable dangling bonds (DBs) are separated by 40 Å and are indistinguishable from the native DBs [3,4]. Hence the simple breaking of a weak silicon bond with two nearby DBs is not viable. Spin-echo measurements indicate that no H atoms occur within a region of ~4 Å around the DB, i.e., an anticorrelation between DB and H. Measurements [5–7] of mobility-lifetime ($\mu\tau$) products infer multiple species of metastable defects with different annealing energies and electron capture cross sections. Metastability has been observed at 4 K temperatures [8]. Branz proposed the H-collision model [9], where the breaking of Si-H bonds, and subsequent diffusion and collision of H, leads to isolated silicon DBs. We propose a distinct new model of the SW effect that unifies several puzzling observations and has rearrangements of the Si network as the essential ingredient. This model has analogies to the H-collision model.

We propose that metastability occurs in three steps: (i) Illumination creates photoexcited electrons and holes. Nonradiative recombination of e-h pairs can break a weak silicon bond and generate a dangling bond–floating bond (FB) pair, analogous to a vacancy-interstitial pair in c-Si. (ii) The mobile FB diffuses away from the location of the DB. (iii) Migrating FBs recombine or annihilate, accompanied by local H rearrangement. Weak silicon bonds are then broken and DBs are created at spatially separated parts of the network. Our detailed calculations support the earlier proposals of Pantelides [10] on the bond-breaking step and formation of FBs. However, our final results for the metastable state are very different.

We find that nonradiative recombination of an e-h pair can break a weak silicon bond. A weak silicon bond (c-d in Fig. 1) can stretch and create a dangling bond on site c. Site d forms a new bond with site x (d-x). Site x is now five-coordinated but d remains four-coordinated. The Frenkel pair of DB and FB is separated by more than 4 Å and stabilized, ($\mathrm{Si}_c - \mathrm{Si}_d + \mathrm{Si}_x - \mathrm{Si}_y \rightarrow \mathrm{Si}_c^* + \mathrm{Si}_d^4 — \mathrm{Si}_x^5 - \mathrm{Si}_y$). The energy barrier to break the weak Si bond has a low value of ~0.85 eV for the ground state of the electronic system [Fig. 1c], similar to the measured activation energy for defect creation [11]. This barrier is much lower than the ~2 eV to break a silicon bond, since the energy cost in breaking bond c-d is compensated by the energy gain in simultaneously forming bond d-x. Calculations utilized tight-binding molecular dynamics that has been very successful for a-Si:H [12].

Nonradiative e-h recombination provides a very low energy path for bond breaking. A weak bond (WB) (e.g., c-d) can easily trap a hole in a band-tail state. A mobile photoexcited electron can be trapped in the vicinity of this hole. The energy barrier for bond breaking in this excited e-h (exciton) state is remarkably lowered to ~0.35 eV

 © 2002 The American Physical Society

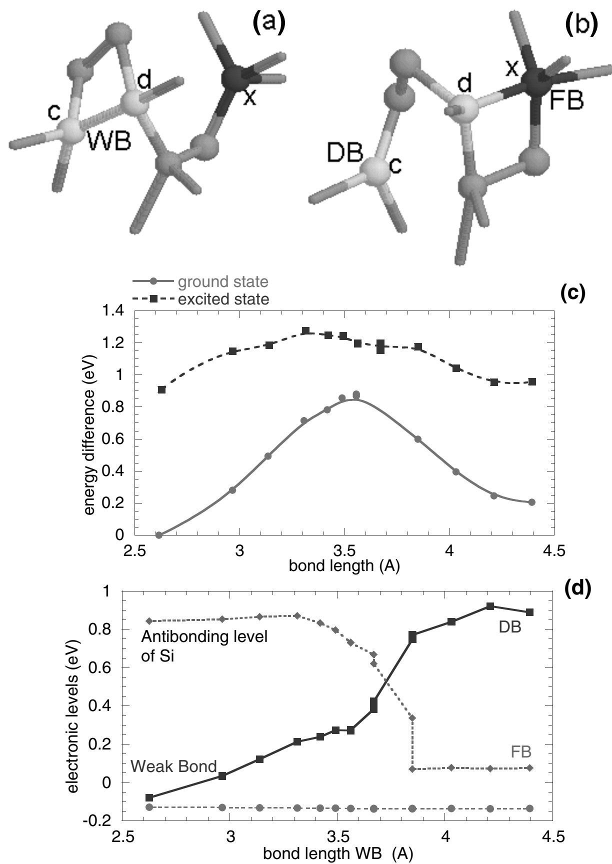

FIG. 1. (a) Portion of a 238 atom a-Si:H cell showing a weak bond (2.62 Å) between atoms c-d. (b) The weak bond has broken, a dangling bond on c and a new bond d-x is created resulting in a floating bond (five-coordinated atom) at x. (c) Calculated total energy as a function of the bond length for the ground state (circles) and e-h pair excited state (squares). (d) The variation in the electronic energy levels in the gap region when the WB is broken and the DB-FB pair is formed. A doubly filled valence band level (circles) is also shown.

[Fig. 1c] due to the crossing of electronic levels in the gap [Fig. 1d]. A thorough search in the configuration space may reduce the energy barrier further.

In the excited state, a hole is initially trapped in the bonding level of the WB and an electron occupies the antibonding level in the conduction band [left side of Fig. 1d]. As the weak bond stretches, the antibonding level lowers in the gap, reducing the barrier similar to a recent calculation [13]. As the WB breaks, the levels cross and both electrons switch to the lower FB level in the valence band tail in the final state [right side of Fig. 1d]. The metastable DB-FB pair has an energy within ~0.2 eV of the initial weak bond state, confirming the earlier proposals on FBs [10,14].

In our models, stretched or distorted Si bonds do not occur in the proximity of a H atom, since the reduced structural constraints at a Si-H site allow the network to be locally more relaxed. Si atoms with large bond-length or bond-angle deviations are a third or farther neighbor from any H. Breaking such WBs produces DBs that are anticorrelated with H and >4 Å away from H. This is a natural explanation of the spin-echo measurements [3,4].

We observed several occurrences of weak silicon bond breaking and generation of DB-FB pairs (Fig. 2), where the initial state had no coordination defects. The energy of the final DB-FB final state and the ground state energy barrier [15] decreases with the Si-bond length (Fig. 2). Statistically, bond lengths elongated more than ~0.25 Å are needed for this process to be energetically favorable. Additionally, adequate volume must be available around the weak bond for the Frenkel pair to be spatially separated.

The second step in defect creation is the migration of the FB. If the created DB and FB recombine, no defects are created. The time for the FB to hop to the next site provides an additional time scale for defect creation. Migration of FBs involves the switching of a bond, without the diffusion of Si atoms. We observed such FB migration events in molecular dynamics simulations on a-Si:H. Atomic displacements during this FB migration process range between 0.2–0.9 Å, far less than displacements (>2 Å) for atomic diffusion.

As mobile FBs migrate the common process is annihilation, where a FB can recombine with an existing Si DB, converting it to a four-coordinated site ($Si^3 + Si^5 \rightarrow Si^4$—$Si^4$). The frequent FB annihilation process occurs when a migrating FB is close to one of the abundant SiH bonds in the network [Fig. 3(a)]. The H moves into the FB site, converting it to a four-coordinated site and a new SiH bond [Fig. 3(b)]. A secondary DB (Si_c^*) can be left behind at the original SiH site, represented by Si^5—$Si^4 + Si_cH \rightarrow Si^4 +$ Si-H $+ Si_c^*$. The FB need not be the nearest neighbor of the SiH. We find several configurations where the H can undergo a local motion to the FB site, resulting in a distance between the DB (Si_c^* or site 54 in Fig. 3) and the H of more than 4–5 Å, consistent with the ESR data. We have found several final configurations with two spatially separated DBs, where the energy difference of the initial and final configuration (e.g., Fig. 3) is less than 0.5 eV. The local motion and rebonding of the

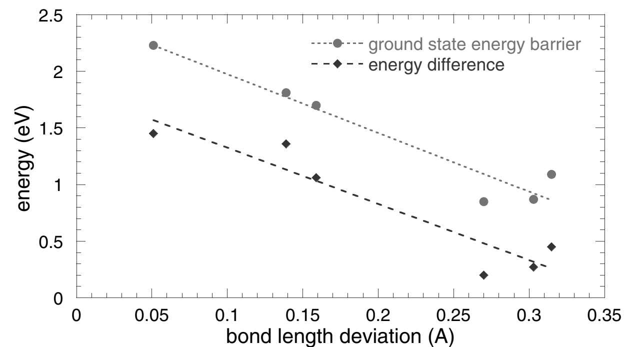

FIG. 2. Calculated energy barrier (circles) and energy of DB-FB configuration (diamonds) and energy barrier (circles) for weak bond breaking, relative to the initial weak bond configuration, as a function of the weak silicon bond length. Dashed best-fit lines are a visual guide.

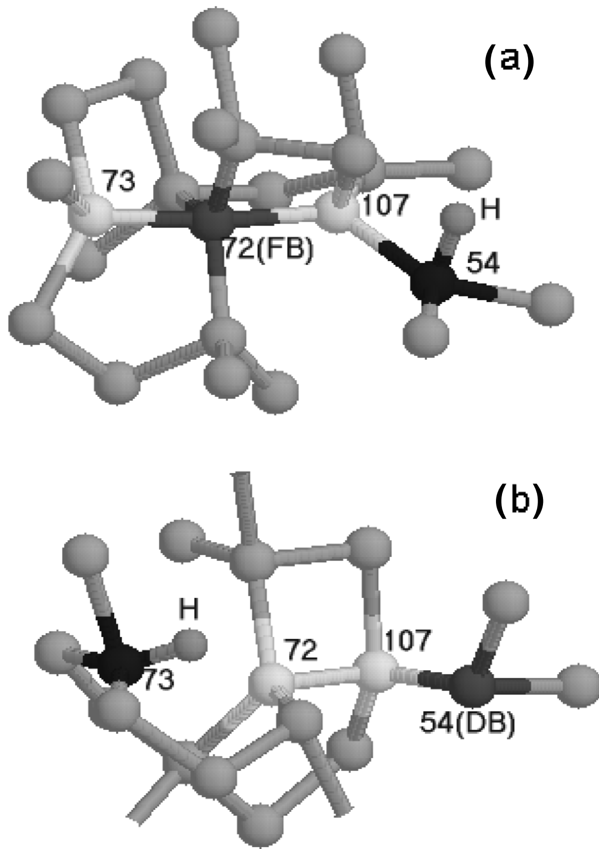

FIG. 3. (a) Initial configuration in a 241 atom a-Si:H cell showing a FB at site 72 close to a SiH bond. (b) The H moves and bonds to 73, converting 72 to a four-coordinated site. Silicon 54 is a dangling bond. Not all bonds of the boundary atoms are shown.

H distinctly differs from long-range H motion in the H-collision model [9]. A weaker annihilation channel is when two migrating FBs are in close proximity and annihilate (Si^5—$Si^5 \rightarrow Si^4 + Si^4$).

The kinetics of defect formation is governed by the competition between the densities of WBs (N_w), DBs (N_{db}), and FBs (N_f). Similar to previous models [2], we assume that the breaking of weak Si bonds and the consequent production of DBs are controlled by the recombination of e-h pairs or the np product at room temperature. Since $n = p = G/N_{db}$, WBs are broken at a rate $k_w(G^2/N_{db}^2)\, N_w$ (k_w is a rate constant), and the DBs are produced (dN_{db}/dt) at the same rate. This immediately leads to the well-known $N \sim k_w G^{2/3} t^{1/3}$ kinetics of DB creation [2]. To connect atomistic results to the continuum case we develop rate equations with additional processes. Diffusing FBs recombine with DBs with a rate $k_r N_{db} N_f$, which decreases N_{db} and N_f but increases N_w. Two diffusing FBs may recombine with a rate $2k_f N_f^2$, and produce new weak bonds at a rate $k_f N_f^2$. The FB-H annihilation is proportional to the H density N_H through $C_1 N_f N_H$. The resulting rate equations are

$$\frac{dN_w}{dt} = -\frac{k_w G^2 N_w}{N_{db}^2} + k_r N_{db} N_f + k_f N_f^2, \qquad (1)$$

$$\frac{dN_{db}}{dt} = \frac{k_w G^2 N_w}{N_{db}^2} - k_r N_{db} N_f + C_1 N_f N_H - D_0 N_m G, \qquad (2)$$

$$\frac{dN_f}{dt} = \frac{k_w G^2 N_w}{N_{db}^2} - k_r N_{db} N_f - 2k_f N_f^2 - C_1 N_f N_H + D_0 N_m G, \qquad (3)$$

$$\frac{dN_m}{dt} = C_1 N_f N_H - D_0 N_m G. \qquad (4)$$

We also include a light-induced annealing term ($D_0 N_m G$) proportional to the light intensity (G) and a subsidiary equation describing the density of locally displaced H (N_m). These rate equations are mathematically similar to the H-collision model [9] since FBs are the analog of mobile H. We have numerically integrated these rate equations with a fourth order Runge-Kutta algorithm. The kinetics of DB formation is very well described by a $t^{1/3}$ power law. As in experiment [16] the DB density saturates at long times (Fig. 4) between 10^{16}–10^{17} cm^{-3}, with a value dependent on the light intensity. The FB density initially rises, then falls as the recombination with H becomes significant and N_f finally saturates near 10^{15} cm^{-3}, much smaller than the DB density, similar to alternative FB models [14].

The rate coefficients used (Table I) were guided by previous simulations [9] and experiments [2]. The product $k_w N_w$ is the SW rate constant C_{sw} that has been experimentally estimated [9] to range between 10–100 cm^{-3} s.

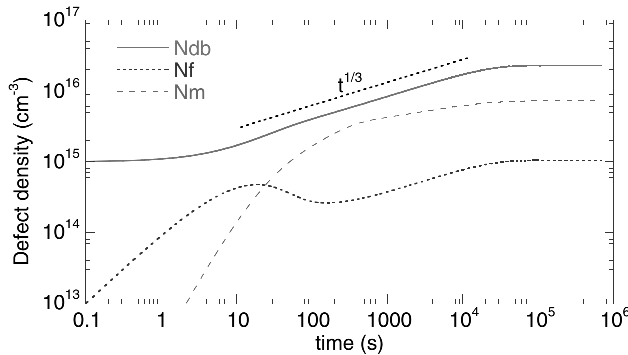

FIG. 4. Increase of the metastable dangling bond density (solid line) from integration of rate equations, showing the comparison with $t^{1/3}$ power law (dashed line), and saturation at long times. The density of FBs N_f (dotted line) and displaced H atoms N_m is also shown.

TABLE I. The values of the rate constants in the kinetic equations.

	Value		Value
$k_w N_w$	100 cm^{-3} s	G	1×10^{21} cm^{-3} s^{-1} (1 sun)
k_w	5×10^{-21} s	D_0	5×10^{-24} cm^3 s^{-1}
N_w	$2 \times 10^{+19}$ cm^{-3}	C_1	1×10^{-23} cm^3 s^{-1}
k_r	8×10^{-21} cm^3 s^{-1}	N_H	5×10^{21} cm^{-3} (10% H)
k_f	8×10^{-21} cm^3 s^{-1}		

k_r and k_f are equal so that the creation term $\frac{k_w G^2 N_w}{N_{db}^2}$ is 3–4 orders larger than the recombination term $k_r N_{db} N_f$ initially ($N_{db}, N_f \sim 10^{15}$ cm^{-3}). This contrains $4 \times 10^{-21} < k_r < 2 \times 10^{-20}$ cm^{-3} s, and early time kinetics is dominated by the creation term. C_1 is chosen to be substantially smaller than k_r, reflecting the expected smaller cross section in displacing H to eliminate FB's. However, the large density of H leads to a numerically large value of $C_1 N_f N_H$ which is counterbalanced by $D_0 N_m G$, setting the value of D_0. If only C_1 is reduced, the FB annihilation is reduced and the saturated value of N_f increases. However, if both the coupled variables C_1 and D_0 are reduced by the same factor, similar solutions as in Fig. 3 are obtained. The qualitative kinetics is robust to small changes of the parameters.

Metastable midgap electronic states arise from the large neutral DB density (D^0), (10^{16}–10^{17} cm^{-3}) and not from the FBs. We find that FBs have filled levels in the valence band, which are doubly occupied and do not contribute to midgap states or the ESR signal. There can be a small residual density of FB (10^{15} cm^{-3}) in the light-soaked state. Because of charge neutrality, the FBs remove charge from DB states, creating an equal number of positively charged DBs (D^+) ($\sim 10^{15}$ cm^{-3})—as suggested by Stradins *et al.* [7]. D^+ defects have a large electron capture cross section acting as primary recombination centers, and cause large changes in the $\mu\tau$ product. The degraded state has a large density of D^0 and a small but equal density of D^+ and negatively charged FBs, supporting observations of charged defects [6]. The D^0 and D^+ may be identified with the two types of defects inferred in recent $\mu\tau$ experiments [5–7]. The steady state defect density and the optical absorption (α) are then dominated by the neutral DB (D^0) (Fig. 3).

We propose that the hysteresis in defect annealing arises from a novel two-step mechanism. First, DBs become mobile at the lower annealing temperature. Negative FBs$^-$ diffuse and annihilate with D^+ defects. Annealing of charged defects creates a small decrease in the total defect density or absorption α, but creates a large increase in $\mu\tau$, explaining the first part of the observed annealing. Second, at a slightly higher temperature, the displaced H begin to diffuse and reduce the remaining large density of neutral DBs, substantially reducing α but only slightly decreasing $\mu\tau$. This model consistently describes, for the first time, the hysteresis of the anneal and the multiple species of defects. Our simulations suggest a lower energy barrier for FB migration than for H motion, and activated computational methods [17] may be necessary for quantification.

At low temperatures ($T \sim 4$ K), where the SW effect is still observed [8], FB mobility and the FB-H interaction may be small (reduced C_1). The kinetics from (1)–(4) lead to larger values of saturated FB densities [$(2–7) \times 10^{15}$ cm^{-3}] than in Fig. 3, together with a small decrease in N_{db}^{sat}. We then predict a larger density of charged DBs (D^+), coupled with FB^- at low temperature, which would be different from room-temperature light soaking.

In summary, metastable defect creation is driven by the breaking of weak silicon bonds and the rebonding of both silicon and H sites. FBs are a transient defect species in this model that should be inhibited in better-ordered samples. Long-range H motion is not required in the defect creation process although it is involved in annealing. This mechanism should be valid in other amorphous semiconductors, where overcoordinated defects can exist, such as amorphous germanium or *a*-SiGe alloys. This new model provides a platform for unifying many unresolved observations of light-induced degradation in amorphous and microcrystalline silicon including charged defects.

We thank H-Y. Lee and W. Hermanto for computational assistance and J. Shinar, H. Branz, J. Clem, and the National Amorphous Thin Film Team for discussions. Acknowledgment is made to the donors of the Petroleum Research Fund administered by the American Chemical Society for support of this research. Support from the NSFC, with Grant No. 69876025 (B. C. P.), and NREL subcontract ACQ-1-30619-08 is acknowledged.

[1] D. L. Staebler and C. R. Wronski, Appl. Phys. Lett. **31**, 292 (1977).
[2] M. Stutzmann, W. B. Jackson, and C. C. Tsai, Phys. Rev. B **32**, 23 (1985).
[3] J. Isoya, S. Yamasaki, H. Okushi, A. Matsuda, and K. Tanaka, Phys. Rev. B **47**, 7013 (1993).
[4] M. S. Brandt, M. S. Bayerl, M. Stutzmann, and C. Graff, J. Non-Cryst. Solids **227-230**, 343 (1998).
[5] D. Han and H. Fritzsche, J. Non-Cryst. Solids **59-60**, 397 (1983).
[6] C. Wronski, Mater. Res. Soc. Symp. Proc. **467**, 7 (1997); R. Koval, X. Niu, J. Pierce, L. Jiao, G. Ganguly, J. Yang, S. Guha, R. W. Collins, and C. Wronski, Mater. Res. Soc. Symp. Proc. **609**, A15.5 (2000).
[7] P. Stradins, S. Shimizu, M. Kondo, and A. Matsuda, Mater. Res. Soc. Symp. Proc. **664**, A12.01 (2001); S. Heck and H. M. Branz, *ibid.* A12.2 (2001).
[8] P. Stradins and H. Fritzsche, Philos. Mag. B **69**, 121 (1994).
[9] H. Branz, Solid State Commun. **105**, 387 (1998); Phys. Rev. B **59**, 5498 (1999).
[10] S. Pantelides, Phys. Rev. Lett. **58**, 1344 (1987); Phys. Rev. B **36**, 3479 (1987).
[11] R. Crandall, Phys. Rev. B **43**, 4057 (1991).
[12] R. Biswas and Y. P. Li, Phys. Rev. Lett. **82**, 2512 (1999).
[13] S. B. Zhang and H. Branz, Phys. Rev. Lett. **84**, 967 (2000).
[14] T. Shimizu and M. Kumeda, Jpn. J. Appl. Phys. **38**, L911 (1998).
[15] Calculations of Fig. 2 include weak bonds in 476–484 atom models and includes the model of U. Hansen and P. Vogl [Phys. Rev. B **57**, 13 295 (1998)].
[16] H. R. Park, J. Z. Liu, and S. Wagner, Appl. Phys. Lett. **55**, 2658 (1989).
[17] G. Barkema and N. Mousseau, Phys. Rev. Lett. **77**, 4358 (1996).